

# PCCP

Accepted Manuscript



This is an *Accepted Manuscript*, which has been through the Royal Society of Chemistry peer review process and has been accepted for publication.

*Accepted Manuscripts* are published online shortly after acceptance, before technical editing, formatting and proof reading. Using this free service, authors can make their results available to the community, in citable form, before we publish the edited article. We will replace this *Accepted Manuscript* with the edited and formatted *Advance Article* as soon as it is available.

You can find more information about *Accepted Manuscripts* in the [Information for Authors](#).

Please note that technical editing may introduce minor changes to the text and/or graphics, which may alter content. The journal's standard [Terms & Conditions](#) and the [Ethical guidelines](#) still apply. In no event shall the Royal Society of Chemistry be held responsible for any errors or omissions in this *Accepted Manuscript* or any consequences arising from the use of any information it contains.

# The interaction of gold and silver nanoparticles with a range of anionic and cationic dyes

Cite this: DOI: 10.1039/x0xx00000x

H. Kitching, A. J. Kenyon and I. P. Parkin\*

Received 00th January 2012,  
Accepted 00th January 2012

DOI: 10.1039/x0xx00000x

[www.rsc.org/](http://www.rsc.org/)

We describe the synthesis of charge-stabilised gold and silver nanoparticles by a modified Turkevich method and their interaction with a selection of cationic and anionic dyes. It was found that gold nanoparticles interact strongly with cationic dyes and in some cases enhanced absorption was observed by UV-visible spectroscopy. It is also shown that addition of cationic dyes to gold nanoparticles triggers aggregation of the nanoparticles into large, micrometre-scale clusters. Simultaneous fragmentation and agglomeration of the gold nanoparticles was observed at high concentrations of cationic dye in the solution. These effects were not observed when gold nanoparticles were mixed with anionic dyes, nor for silver nanoparticles with either cationic or anionic dyes.

## Introduction

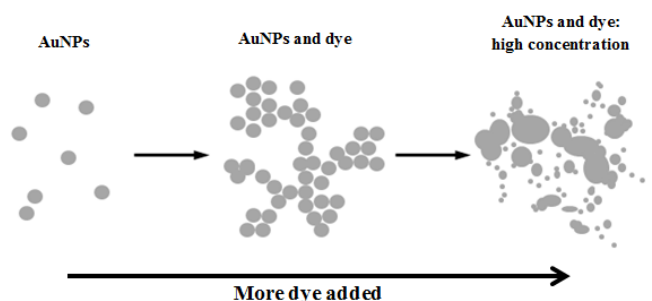
An explosion in the number of infections caused by antibiotic-resistant strains of bacteria such as *Staphylococcus aureus* and *Mycobacterium tuberculosis* has become a huge problem over the last few decades.<sup>1</sup> New, alternative treatments are required to treat these dangerous drug-resistant pathogens when standard antibiotic therapies fail. One potential treatment is photodynamic therapy (PDT), which can be used to kill bacterial or somatic cells for cancer therapies.<sup>2</sup> When exposed to a specific frequency of light a photosensitizer absorbs a photon and is promoted to a high-energy triplet state. The excited state of the photosensitizer then interacts with an oxygen molecule and generates singlet oxygen. This is a highly cytotoxic species that can kill cells by damaging both cell walls and DNA.<sup>3</sup>

There are several well-known groups of photosensitizers available including porphyrins, chlorophylls, and dyes.<sup>4</sup> Thiazines, a family of dyes most often used as biological stains, are commonly used as photosensitizers. This family includes methylene blue, toluidine blue, thionin and azures A, B and C and there have already been studies showing their efficacy as photosensitizers.<sup>5, 6</sup> It has been shown that a topical application of methylene blue to a wound infected with epidemic methicillin-resistant *Staphylococcus aureus* (EMRSA), followed by illumination by 670 nm light produces a 25-fold reduction in the number of viable EMRSA bacteria.<sup>7</sup> Methylene blue has also proved to be effective against *E. coli*<sup>8</sup> and cancer cells.<sup>9</sup> Targeted *in vivo* killing of tumour cells with little damage to healthy surrounding tissues is also a possibility if the photosensitizer can be coupled to a microbe-recognising moiety.<sup>9</sup>

The efficacy of photosensitizing agents can be greatly increased by forming a conjugate with a nanomaterial.<sup>10, 11</sup> Narband *et al.* reported that the toluidine blue-induced lethal photosensitization of *Staphylococcus aureus* can be increased by conjugation with gold nanoparticles. Enormous enhancements of kills by an order of one order of magnitude were observed compared to using toluidine blue alone as a photosensitiser.<sup>12</sup> Further studies on this system showed that gold nanoparticles enhanced the UV-visible absorption of toluidine blue and other thiazine dyes at a specific concentration, producing up to a ten-fold increase in the extinction coefficient of a dye-only solution at comparable concentrations.<sup>12</sup>

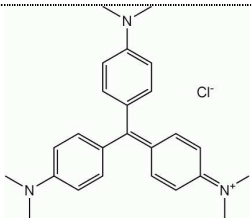
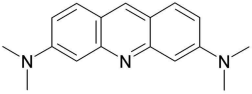
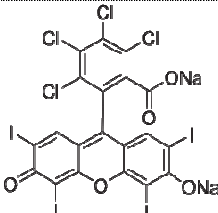
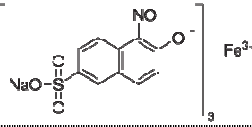
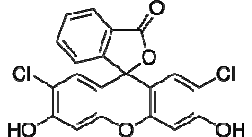
Here we report on the interaction of gold and silver nanoparticles synthesised by a modified Turkevich method<sup>13</sup> with a range of cationic and anionic dyes (**Table 1**). It is found that all the cationic dyes used in this study interact strongly with the gold nanoparticles and cause them to aggregate together into large arrays. Enhanced absorption of the dye at a critical concentration is observed for toluidine blue, crystal violet and acridine orange. Fragmentation of the nanoparticles into smaller pieces and larger, non-spherical particles was also observed at high concentrations of dye in the nanoparticle solutions (**Scheme 1**). No interaction of cationic or anionic dyes was observed with silver nanoparticles.

**Scheme 1** An overview of the processes observed during the titration of cationic dyes with a solution of gold nanoparticles.



**Table 1** Dyes used in the titration experiments, their structures and concentrations.

Dye	Structure	Concentration ( $\mu\text{M}$ )
<i>Cationic dyes</i>		
Toluidine Blue O		5
Malachite Green		20
Rhodamine 6G		20

Crystal Violet		5
Acridine Orange		20
<i>Anionic dyes</i>		
Rose Bengal		20
Naphthol Green B		20
2',7'-Dichlorofluorescein		20

## Experimental methods

Stock solutions were made up as below:

**Solution A:**  $\text{HAuCl}_4 \cdot 3\text{H}_2\text{O}$  (49.2 mg, 0.125 mmol) was dissolved in deionised water (25 mL) giving a 5 mM solution.

**Solution B:**  $\text{AgNO}_3$  (45 mg, 0.26 mmol) was dissolved in deionised water (50 mL) to form an approximately 5 mM solution.

**Solution C:**  $\text{Na}_3\text{C}_6\text{H}_5\text{O}_7 \cdot 2\text{H}_2\text{O}$  (294.7 mg, 1 mmol) was dissolved in deionised water (50 mL) giving a 20 mM solution.

### Synthesis of charge-stabilised gold nanoparticles

**Solution A** (1 mL) was dissolved in deionised water (18 mL) and heated. Mixture was boiled for 2 min. **Solution C** (1 mL) was added dropwise over ~45 s. The mixture was boiled for a further 1 min then removed from the heat and allowed to cool. A colour change from colourless to lilac to pinkish red to a bright scarlet was observed. Cooled nanoparticle solutions were used in titration experiments with dyes, as described below.

### Synthesis of charge-stabilised silver nanoparticles

**Solution B** (1 mL) was dissolved in deionised water (18 mL) and heated. The mixture was boiled for 2 min. **Solution C** (1 mL) was added dropwise over ~45 s. The mixture was refluxed for 30 min then allowed to cool. A gradual colour change was observed from colourless to yellowish-white was observed. Cooled nanoparticle solutions were used in titration experiments with dyes, as described below.

### Titration experiments

Dye solutions were made up by dissolving a known mass of the solid dye in deionised water. The list of dyes used in these experiments, their structures and respective concentrations can be found in **Table 1**.

UV-visible (UV-vis) spectra of nanoparticle solutions and dye solution were obtained separately. Dye solution (1 mL) was then added to the nanoparticle solution (16 mL) and stirred. A cuvette was filled with the mixture and the UV-vis spectrum obtained. The solution was not discarded but poured back into the original mixture. A further 1 mL of dye solution was added and the process repeated. This was repeated 15 times, using 15 mL of dye solution in total.

### UV-visible absorption measurements

UV-visible absorption spectra were recorded on a Shimadzu UV-1800 Spectrophotometer. Plastic cuvettes with a path length of 10 mm were used. Absorption was measured over the spectral range 200 – 1000 nm.

### Particle size measurements

Using a Zetasizer 3000 (Malvern, UK), photon correlation spectroscopy was used to measure the hydrodynamic radius of the gold nanoparticles before and during titration experiments. Experiments were carried out at 25 °C using plastic cuvettes.

Transmission electron microscopy (TEM) was used to study the size of the gold nanoparticles both before and during the titration experiments. Samples of the gold nanoparticles without dyes were prepared by allowing drops of nanoparticle solution to evaporate onto carbon coated copper grids. Samples were also taken at various points in the titration experiments when dye solution had been added to the nanoparticles so the effect of adding dyes on the nanoparticle size and distribution could be observed and compared to the nanoparticle-only sample.

## Results and discussion

### UV-vis absorption studies

During titration experiments with gold nanoparticles all of the cationic dyes studied exhibited formation of a new peak at approximately 630 – 690 nm. Formation of a new peak, separate to those corresponding to the dye and the nanoparticles independently and found at a large (~100 nm) red shift, was indicative of aggregation of the nanoparticles into large arrays. This deduction is confirmed by particle size measurements, discussed later. This effect was more marked for some cationic dyes than others. The UV-vis spectrum of malachite green titrated with gold nanoparticles (**Figure 1**) showed only a small shoulder at 685 nm. It is possible that some of the absorption at 685 nm is being masked by overlap with the absorption of the dye peak, which for malachite green is found at 617 nm in relative proximity to the aggregate peak. However, TEM analysis for this sample (shown later in **Figure 16**) shows limited aggregation, explaining the lack of intensity in the aggregation peak.

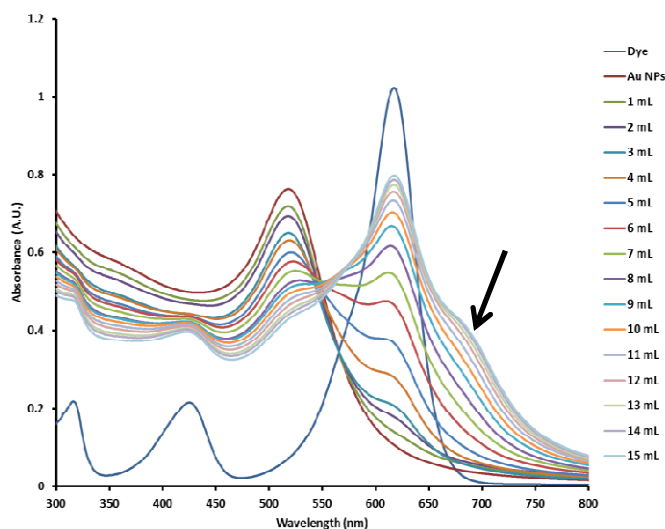


**Figure 1** UV-vis absorption spectra of malachite green in a solution of gold nanoparticles. ‘Dye’ corresponds to the absorption spectrum of 20  $\mu$ M malachite green dye on its own; ‘Au NPs’ to the absorption spectrum of 5 mM gold nanoparticle solution only. ‘1 mL’ corresponds to the absorption spectrum of 1 mL 20  $\mu$ M malachite green in 16 mL 5 mM gold nanoparticle solution. 2 mL corresponds to the absorption spectrum of 2 mL malachite green in 16 mL nanoparticle solution etc. Shoulder indicative of aggregation is indicated by the black arrow.

Rhodamine 6G titrated with gold nanoparticles showed a new peak forming at 640 nm indicative of aggregation in a similar way (**Figure 2**). However, due to the dye absorption maxima being located much further from the aggregation peak than in malachite

green (527 nm compared to 617 nm) a much clearer, much more distinct peak is observed. This new peak reached maximum absorption after 6 mL of rhodamine 6G had been added to the nanoparticle solution. Increasing dye concentration further caused a decrease in absorption at 640 nm and a very slight red shift, suggesting further minimal aggregation. The decrease in intensity of this peak was simply due to the decreased number of aggregates in solution: as they continue to grow, there are fewer of them.

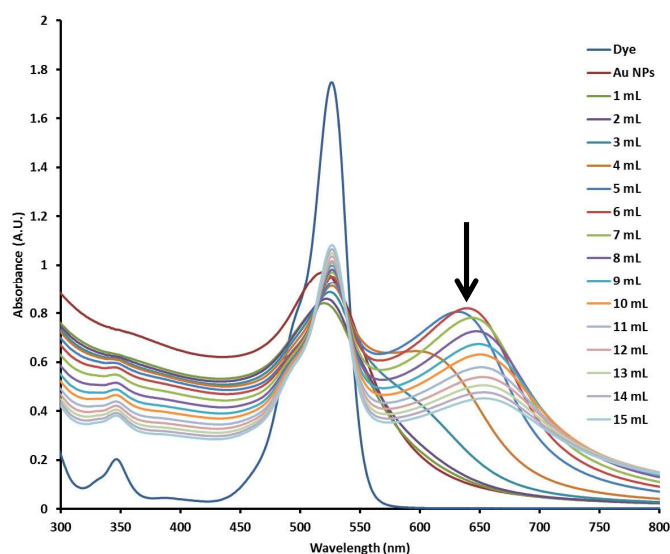


**Figure 2** UV-vis absorption spectra of rhodamine 6G in a solution of gold nanoparticles. ‘Dye’ corresponds to the absorption spectrum of 20  $\mu$ M rhodamine dye on its own; ‘Au NPs’ to the absorption spectrum of 5 mM gold nanoparticle solution only. ‘1 mL’ corresponds to the absorption spectrum of 1 mL 20  $\mu$ M rhodamine in 16 mL 5 mM gold nanoparticle solution. 2 mL corresponds to the absorption spectrum of 2 mL rhodamine in 16 mL nanoparticle solution etc. The peak that forms as nanoparticles aggregate is indicated by a black arrow.

The remaining three cationic dyes in this study show similar features in their UV-vis absorption spectra. However, unlike malachite green and rhodamine 6G, enhanced absorption of the aggregation peak (above the intensity of the dye peak alone) was observed.

The absorption spectra of gold nanoparticles and toluidine blue (**Figure 3**) show enhanced absorption at a critical concentration, as previously reported in the literature<sup>12, 14</sup>. Alongside the expected dilution of the gold nanoparticle surface plasmon resonance (SPR) peak due the decreasing concentration of gold nanoparticles in the overall solution as more dye solution is added (indicated by a grey arrow in **Figure 3**), enhancement of the absorption at 630 nm was observed. Maximum enhancement was observed after 6 mL of toluidine blue had been added, corresponding to a concentration of

dye in the reaction solution of 1.36  $\mu\text{M}$ . Each aliquot thereafter resulted in a decrease in the intensity of the absorption of the dye and a small red shift, as in the spectrum for rhodamine 6G. This enhancement is likely due to the almost perfect overlap of the dye maximum (630 nm) with the absorption corresponding to aggregates of nanoparticles – for this system, also found at 630 nm.

The concentrations of toluidine blue and gold nanoparticles at the point where maximum dye absorption enhancement was observed were calculated to be 1.36  $\mu\text{M}$  and 3.63 mM respectively. Solutions of these concentrations were made up and the UV-vis absorption spectra of each taken separately. The two curves were then mathematically combined, giving the absorption spectrum that would be expected if the nanoparticles and dyes showed no interaction with each other. This is compared with the enhanced absorption observed during the titration experiments described above. This comparison is shown in **Figure 4**. It is clearly seen that the enhanced absorption (purple line) has a higher maximum absorption (0.74 A. U.) than the calculated absorption spectrum of solutions of identical concentration (0.23 A. U.). This is enhancement by a factor of 3, the largest we recorded. It is also seen that the experimentally observed curve is a markedly different shape compared to the calculated spectrum (green line). We clearly see a decreased absorption at 520 nm due to consumption of the original single, well-dispersed gold nanoparticles to form aggregates at 630 nm.

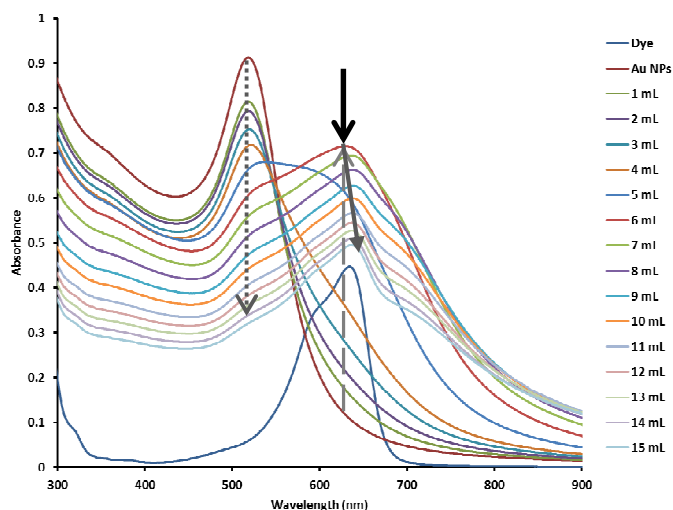


**Figure 3** UV-vis absorption spectra of toluidine blue in a solution of gold nanoparticles. ‘Dye’ corresponds to the absorption spectrum of 5  $\mu\text{M}$  toluidine blue dye on its own; ‘Au NPs’ to the absorption spectrum of 5 mM gold nanoparticle solution only. ‘1 mL’ corresponds to the absorption spectrum of 1 mL 5  $\mu\text{M}$  toluidine blue

in 16 mL 5 mM gold nanoparticle solution. 2 mL corresponds to the absorption spectrum of 2 mL toluidine blue in 16 mL nanoparticles, etc. Black arrow indicates maximum enhancement of the absorption after 6 mL of toluidine blue had been added. Dotted grey arrow indicates decrease in absorbance of the nanoparticle peak as a function of dilution; dashed grey line shows the increase in absorbance of the dye from the start of the experiment to the enhanced absorption observed at 6 mL dye added. Solid grey arrow shows the decrease in intensity and slight red shift of the aggregation peak as further aliquots of toluidine blue after 6 mL are added.

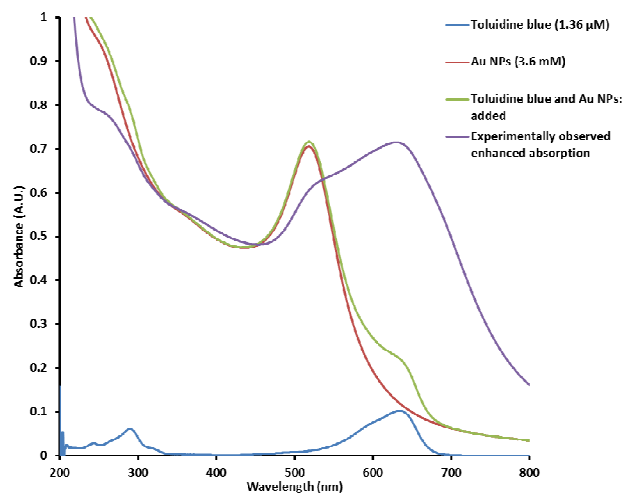


**Figure 4** Graph comparing the UV-vis absorption spectra of toluidine blue at 1.36  $\mu\text{M}$  (blue line), gold nanoparticle solution at 3.63 mM (red line), the spectra of toluidine blue (1.36  $\mu\text{M}$ ) and gold nanoparticle solution (3.63 mM) added together to give a mathematical estimate of the absorption spectrum that could be expected if there were no electronic interaction between toluidine blue and the gold particles (green line), and finally the enhanced absorption of toluidine observed experimentally (purple line).

Similar results were seen during the titration experiment between gold nanoparticles and a solution of crystal violet (**Figure 5**). As crystal violet was added a shoulder began to emerge and develop into a peak at a large red shift. Maximum enhanced absorption at 680 nm was observed after 7 mL of dye solution had been added to the 16 mL of gold nanoparticle solution. This was suggestive of aggregates of nanoparticles forming, as in the other samples. Further aliquots after this critical point resulted in a decrease of the absorption and slight red shift to  $\sim 700$  nm, as seen in the toluidine blue-gold nanoparticle experiment. The concentrations of crystal violet and gold nanoparticles at the critical point where maximum dye absorption enhancement was observed were calculated to be 1.52  $\mu\text{M}$  and 3.48 mM respectively.

Similar results were obtained when titration experiments were carried out using acridine orange (**Figure 6**). An aggregation peak formed at 630 nm and maximum enhancement was observed only 3 mL of acridine orange had been added to the nanoparticles.

The intensity of the aggregation peak was higher than the maximum absorption of the dye alone. Aliquots of acridine orange added after 3 mL caused red shift and a decrease in the intensity of the aggregation peak. A general scheme of what is observed when a cationic dye is added to a solution of gold nanoparticles is given in Scheme 2.

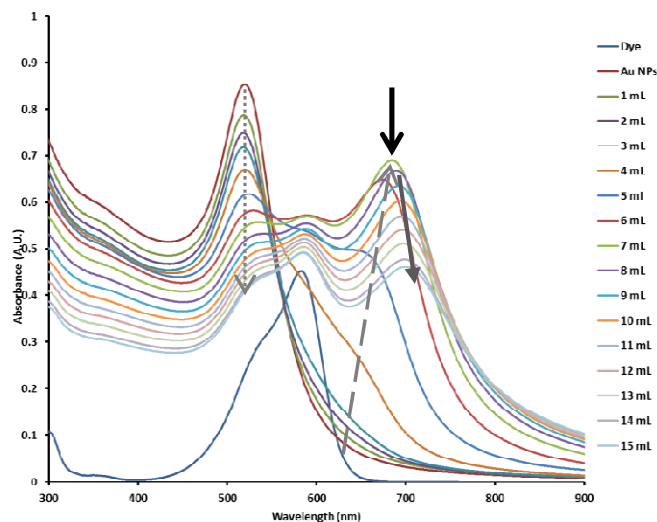


**Figure 5** UV-vis absorption spectra of crystal violet in a solution of gold nanoparticles. Maximum enhancement of the absorption after 7 mL crystal violet had been added is indicated by a black arrow. Grey dotted arrow shows the decrease in absorption of the nanoparticles as a function of dilution; dashed grey arrow shows the increase in absorption of the dye from the start of the experiment to the enhanced absorption observed at 7 mL dye added. Solid grey arrow shows the decrease in intensity and slight red shift of the aggregation peak as further aliquots of crystal violet after 7 mL are added.

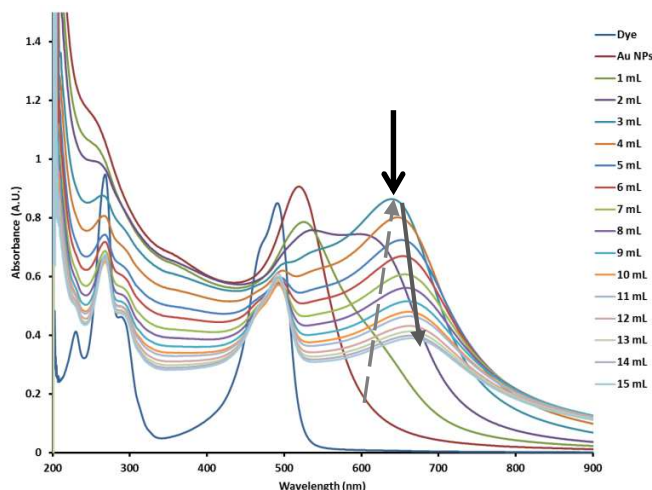


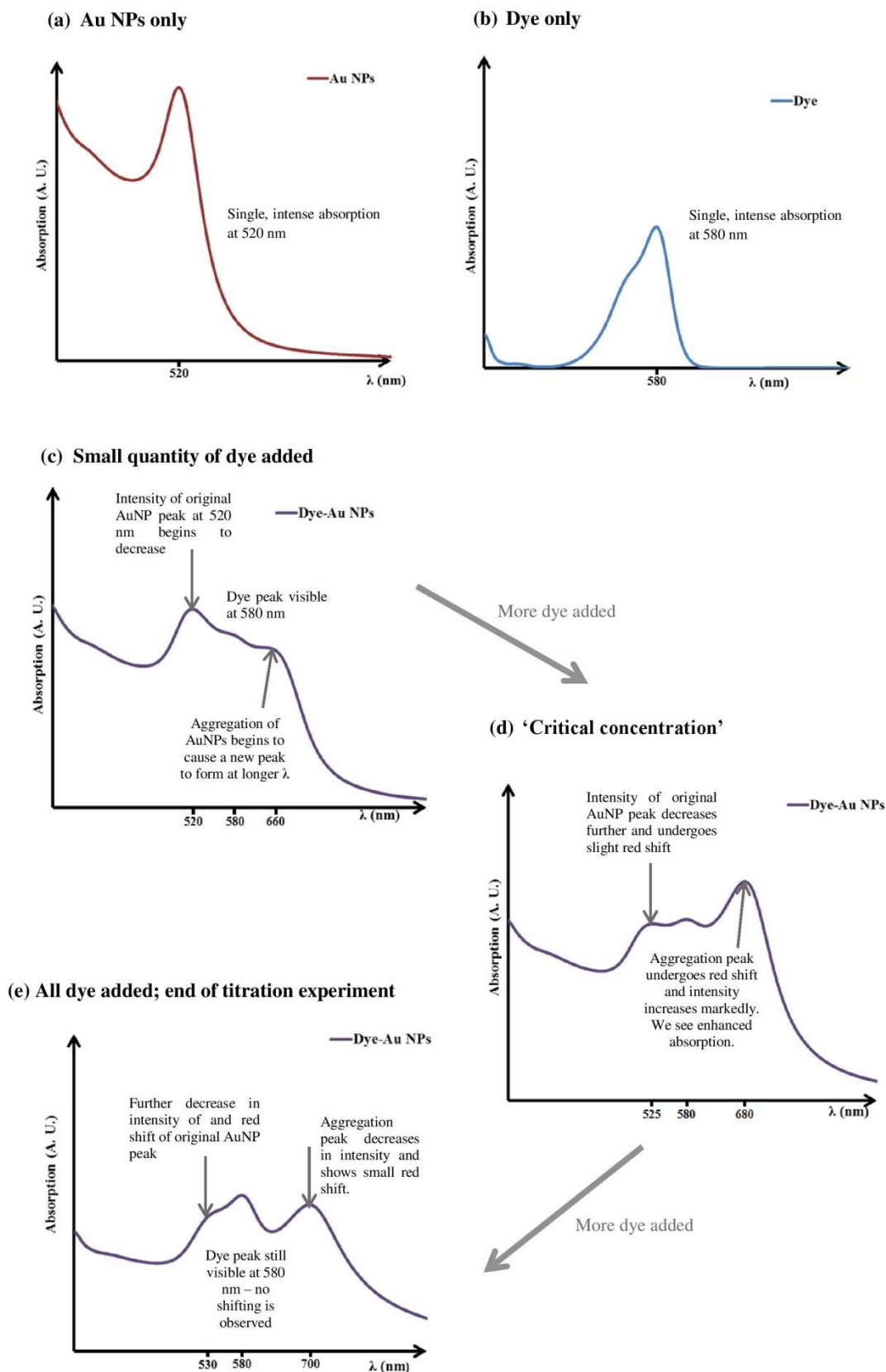
**Figure 6** UV-vis absorption spectra of acridine orange with a solution of gold nanoparticles. Black arrow indicates the new peak that forms after 3 aliquots of acridine orange have been added. Dashed grey arrow shows the increase in absorption and red shift

from the start of the experiment to the enhanced absorption observed at 3 mL dye added. Solid grey arrow shows the decrease in intensity and slight red shift of the aggregation peak as further aliquots of acridine orange after 3 mL are added.

In the case of toluidine blue and crystal violet the dye absorption maxima lie close to the aggregation peak. The maximum absorbance for toluidine blue alone is found at 630 nm which perfectly overlaps the aggregation peak that forms. In this case then we do not see a 'new' peak forming in the UV-vis, merely an enhancement of the absorption as the aggregation peak steals intensity from the dye peak. Similarly, crystal violet's maximum absorption is located at 578 nm, close to the aggregation peak at 685 nm. In this case we do see the aggregation peak emerge separately as it is not masked by the dye absorption, but the two lie sufficiently close that the aggregation peak 'borrows' some intensity from the dye peak to produce the enhanced absorption we observe.

Spectra with no enhancement of absorption and no interaction between the dye molecules and gold nanoparticles were observed for the anionic dyes rose bengal (**Figure 7**), naphthol green (**Figure 8**) and 2',7'-dichlorofluorescein (**Figure 9**) used in this work. All three spectra show the expected decrease in intensity of the nanoparticle peak as the titration experiment progresses as a function of dilution and increase in the intensity of the dye absorption as it becomes more concentrated in the titration mixture. None show extra peaks forming at longer wavelengths that would indicate aggregation of the particles, nor do they show any enhancement of the dye absorption. The spectra of gold nanoparticles with rose bengal and naphthol green show isosbestic points, which are indicative of zero electronic interaction between the particle and the dye molecules. Lack of interaction between these anionic dyes and gold nanoparticles does, however, indicate that the observed agglomeration of gold nanoparticles is not solely due to increasing the ionic strength of the solution as has previously been suggested.<sup>14, 15</sup> If this were the case then anionic dyes should trigger aggregation in a similar manner to the cationic. Presumably, then, the charge on the dye molecules and the way they interact with the surface of the nanoparticle or the citrate shell is also important, and the electrostatic repulsion between the negatively charged anionic dyes and the negatively charged citrate layer on the gold nanoparticles prevents them from coming close enough to aggregate. Under this assumption the positively charged cationic dyes would be attracted to the citrate shell of the nanoparticles, undergo ligand exchange and coordinate with the gold surface. They could potentially act as linker-type molecules, chelating numerous nanoparticles and forming the large aggregates observed.

**Scheme 2** A generalised scheme depicting the changes observed in the UV-vis spectra as a cationic dye is added to a solution of gold nanoparticles. Arrows on spectra indicate general trends observed in peak intensity and red shift.



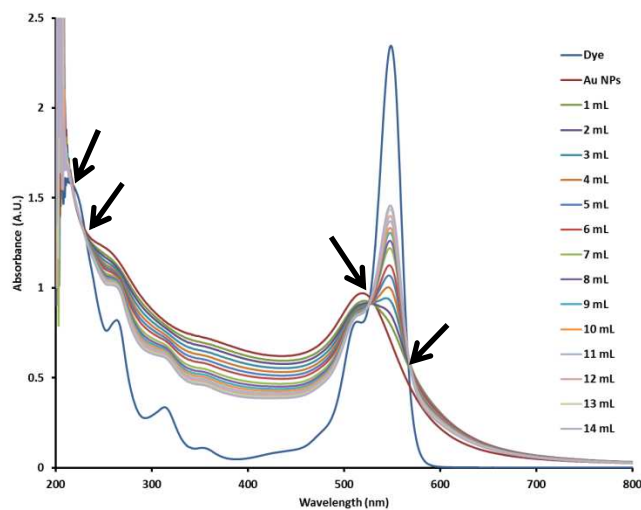


**Figure 7** UV-vis absorption spectra of rose bengal with a solution of gold nanoparticles. Isosbestic points are indicated by black arrows.

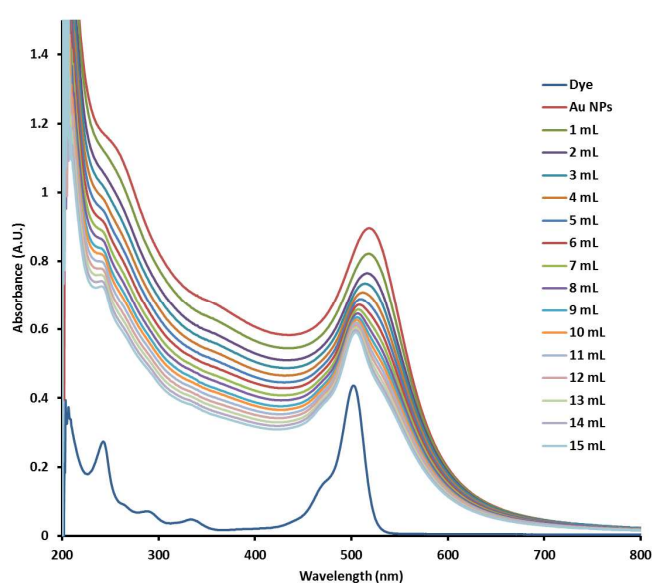


**Figure 9** UV-vis absorption spectra of 2',7'-dichlorofluorescein with a solution of gold nanoparticles.

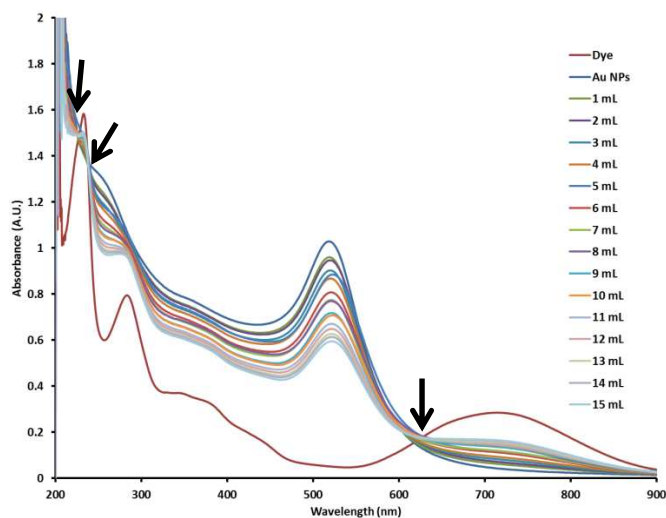


**Figure 8** UV-vis absorption spectra of naphthol green with a solution of gold nanoparticles. Isosbestic points are indicated by black arrows.

Titration of the three anionic dyes with silver nanoparticles also showed no electronic interaction with well-formed isosbestic points being observed (sample spectrum of naphthol green with silver nanoparticles is shown in **Figure 10**). Interestingly, however, titration experiments using silver nanoparticles and cationic dyes also produced UV-vis spectra with no enhanced absorption and a series of clearly formed isosbestic points (**Figure 11** and **12** show the spectra of silver nanoparticles with malachite green and crystal violet respectively), indicating no electronic interaction in these cases too.

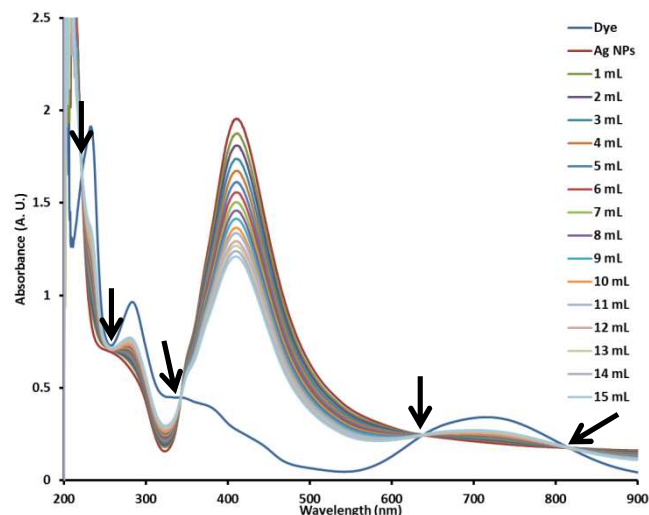


**Figure 10** UV-vis absorption spectra of naphthol green with a solution of silver nanoparticles. Isosbestic points are indicated by black arrows.

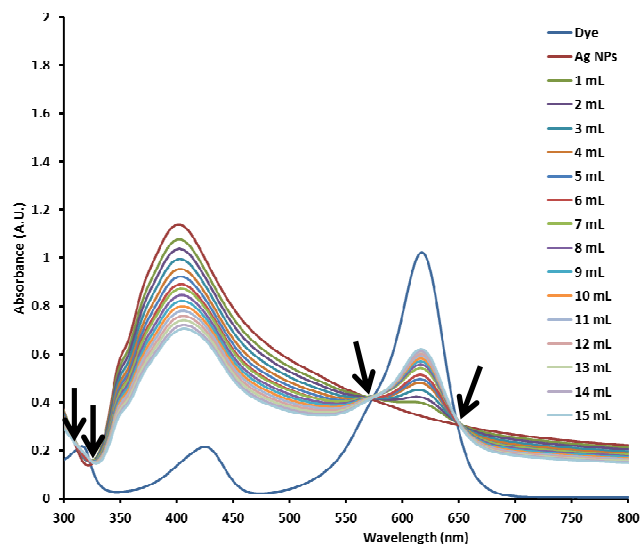


**Figure 11** UV-vis absorption spectra of malachite green with a solution of silver nanoparticles. Isosbestic points are indicated by black arrows.

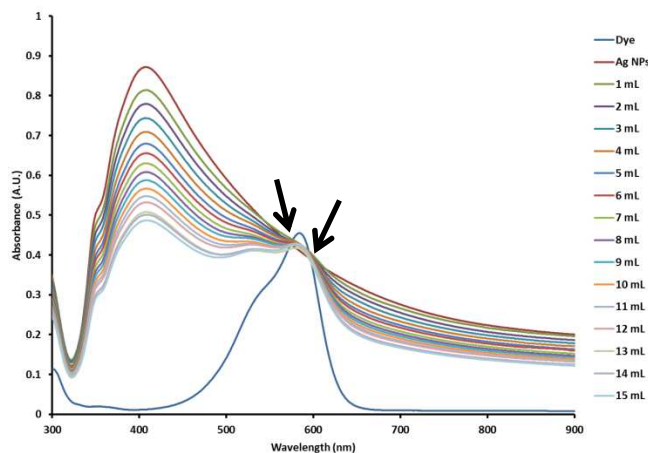


**Figure 12** UV-vis absorption spectra of crystal violet and a solution of silver nanoparticles. Isosbestic points are indicated by black arrows.

It is unclear why aggregation and enhancement of absorption was observed for cationic dyes only when titrated with gold nanoparticles and not with silver. The Turkevich method used to synthesize the particles of both metals produces a nanoparticle with a positive surface charge, stabilised by negatively-charged citrate ions for both silver and gold. Theoretically the similar structures should produce analogous behavior from the gold and silver particles.

Although undetermined at present, it is thought likely that the dyes interact with the surface of the nanoparticle *via* the amine group (all the cationic dyes used in this study have amine groups in common). Amine groups are known to be weakly aurophilic.<sup>16, 17</sup> It has also been reported that silver-amine complexes are less stable than gold-amine species due to the comparatively lower affinity of amines for silver.<sup>18</sup> Furthermore the stabilising citrate ligands coordinate to the metal through a carboxylate group. The binding energy of the carboxylate group to gold clusters is reported to be  $\sim 8$  kJ mol<sup>-1</sup> compared to  $\sim 33$  kJ mol<sup>-1</sup> for amine-gold interactions.<sup>19</sup> Although quantitative data could not be found, it is reported that silver nanoparticles will preferentially bind oxygen-containing ligands (such as citrate) over amine groups.<sup>20</sup> It could be that the lower affinity of amine groups for silver is simply not enough to overcome the stronger Ag-O attraction and therefore the dyes cannot replace the citrate ligands, whereas ligand exchange can occur for gold particles where the relative stability of the gold-citrate complexes is lower.

Alternatively, as toluidine blue is a thiazine it is also possible in this case that the dye molecule is interacting or bonding through the sulphur atoms – sulphur is well known to be exceptionally aurophilic,<sup>21, 22</sup> and this could explain the large enhancement observed in the UV-vis spectrum of gold and toluidine blue.

However, sulphur has also been reported to be argentophilic, so if this is true it does not explain the complete failure of toluidine blue to interact with the silver nanoparticles in any way.<sup>23</sup>

Whether the dyes are coordinating through a nitrogen or sulphur atom, it has not been established whether the interaction is fully electrostatic. It is possible that the silver nanoparticles could have a slightly lower surface charge or may be partially oxidised, impinging on their ability to interact with dye molecules to the same extent.

#### Particle size measurements: TEM studies and Zetasizer

TEM studies of the charge-stabilised gold nanoparticles on their own showed well-formed particles that were predominantly spherical in shape (shown in **Figure 13a**). Particle diameter fell within the range 10-15 nm, with an average diameter of 11 nm observed. TEM images of gold particles before addition of dye solutions showed well distributed particles, predominantly arranged singly or in small groups. This agrees well with the data obtained from the Zetasizer for a sample of the gold nanoparticles, where the average hydrodynamic diameter was found to be 20.5 nm. Particle diameter is typically half the hydrodynamic diameter, corresponding to an average gold nanoparticle size between 10 and 11 nm.

TEM images of silver nanoparticles showed less regularly shaped particles that varied in size from 5-40 nm. A larger variation in particle size is known to occur when silver nanoparticles are synthesised in this way compared to gold.<sup>24</sup>

TEM images of samples after cationic dye solutions had been added to the gold nanoparticles showed some significant differences to those of the nanoparticles alone. Images taken of a nanoparticle solution to which 4 mL of toluidine blue had been added showed significant aggregation of the particles (**Figure 13b**). These arrays were consistently several hundred nanometres across, consisting of hundreds of particles in close proximity, though there were still large numbers of nanoparticles dotted around singly and in small groups. After 5 mL of toluidine blue had been added the observed aggregates were several micrometres across in size (**Figure 13c**). 6 mL of toluidine blue (the critical concentration at which the maximum enhanced absorption of the dye was observed on the UV-vis absorption spectra) showed nanoparticles in huge, multi-micrometre diameter arrays (**Figure 13d**). In contrast to the well-defined particles seen in the other samples, the particles in this were in a globular matrix that appeared rather like frogspawn. Some individual particles appeared to have broken down into smaller, less distinct fragments to form a 'jelly' that larger particles were embedded in. This increase in perceived particle size as the concentration of dye in the system increases is corroborated by the Zetasizer data (**Figure**

**18**), which clearly shows a sharp increase in hydrodynamic radius of the particles in solution after 5 mL of toluidine blue had been added to the nanoparticle solution.

The formation of these large aggregates agrees with the observations made during the UV-vis studies. The spectra obtained for the nanoparticles and 4, 5 and 6 mL of toluidine blue solution mixtures, respectively, show a peak developing at longer wavelengths compared to the peak for Au NPs alone. (630 nm in this case - the same as the absorption of toluidine blue dye alone). This shift to longer wavelengths corresponds to an increase in perceived particle size as reported in the literature.<sup>25</sup>

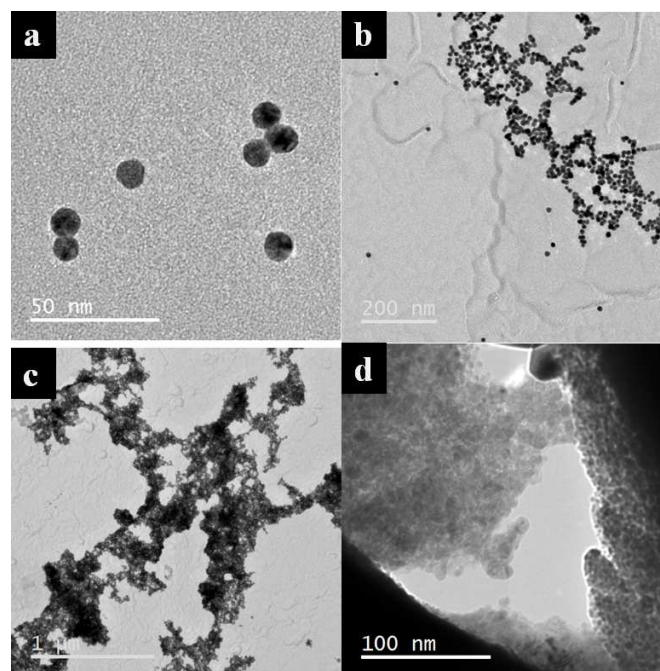


**Figure 13** TEM images showing (a) gold nanoparticles made by the Turkevich method before dye solutions were added; (b) gold nanoparticles to which 4 mL of toluidine blue had been added; (c) gold nanoparticles to which 5 mL toluidine blue had been added; (d) gold nanoparticles to which 6 mL toluidine blue had been added.

TEM studies for crystal violet showed similar results. As more crystal violet was added to the gold nanoparticles aggregation occurred. **Figure 14a** shows gold nanoparticles with 3 mL crystal violet added, well below the critical concentration at which the aggregation peak reaches maximum intensity in the UV-vis spectrum. At this concentration of dye in the nanoparticle solution the nanoparticles remain largely separate and in small groups. **Figure 14b** shows the same system with 6 mL crystal violet added. It can be seen clearly that the nanoparticles are beginning to aggregate together into arrays. These arrays were typically several hundred nanometres across and consisted of closely-spaced but

discrete particles. Further aliquots of crystal violet (10 mL added) cause the aggregates to grow larger, up to a micron in diameter (Figure 14c and d). This is consistent with the red shift seen in the UV-vis. It can be seen that the particles are again beginning to break down into smaller fragments or sinter together to become less well shaped and defined, as in the toluidine blue system. The ‘jelly’-like matrix seen in the TEM images of toluidine blue is not observed in the crystal violet images. Zetasizer data corroborates with these observations, showing an increase in effective particle size from 5 mL crystal violet added onwards.

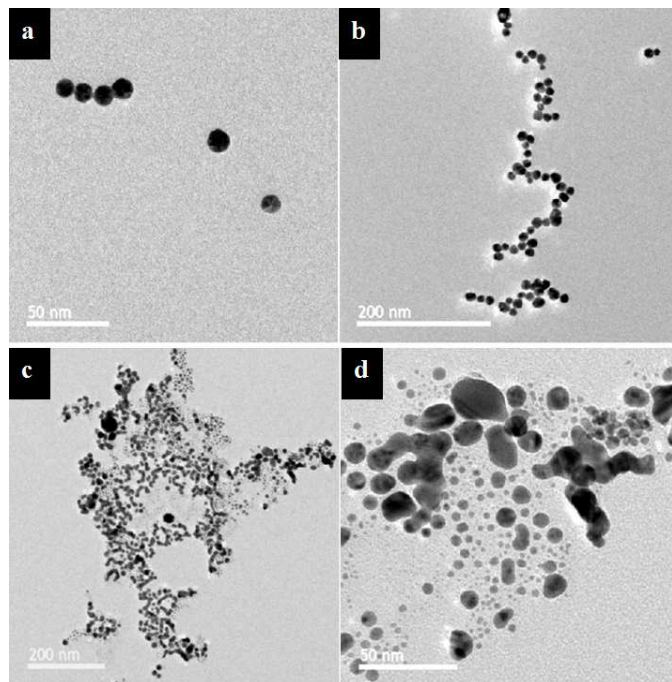


**Figure 14** TEM images showing the formation of aggregates as crystal violet is added to a solution of gold nanoparticles: (a) 3 mL crystal violet added; (b) 6 mL crystal violet added; (c) and (d) 10 mL crystal violet added.

Very similar results were obtained for acridine orange (Figure 15). At the critical concentration (for acridine orange, after 3 aliquots of dye had been added) large aggregates of nanoparticles form extending over several micrometres (Figure 15b). As dye continued to be added particles began to break down into smaller fragments and formed areas of ‘cloudy’ particles (Figure 15c and d). Hydrodynamic radius is seen to increase greatly over the course of the titration experiment, beginning after 2 mL acridine orange had been added (Figure 17), agreeing strongly with the observations made under TEM.

It is unclear why the nanoparticles begin to fragment and become globular as the concentration of these dyes in the nanoparticle solution increases. Loss of the citrate shell as the particles undergo ligand exchange with the dye molecules could cause destabilisation of the surface and subsequent fusion of the nanoparticles, though further work is required to establish if this is the case.

TEM images showing gold nanoparticles mixed with malachite green show some aggregation but to a lesser extent (Figure 16), consistent with the UV-vis data on this system where a small shoulder corresponding to aggregation was observed rather than a large peak. Zetasizer studies showed a small amount of aggregation at high concentrations of malachite green but to a lesser degree than any of the three dyes that show enhancement – the maximum z-average size observed for malachite green was 583 nm, compared to 1654, 1382 and 2230 nm for toluidine blue, crystal violet and acridine orange respectively.

To the best of our knowledge TEM and Zetasizer analysis of the interaction of dyes with gold nanoparticles and observation of the aggregation that occurs has not been reported previously.

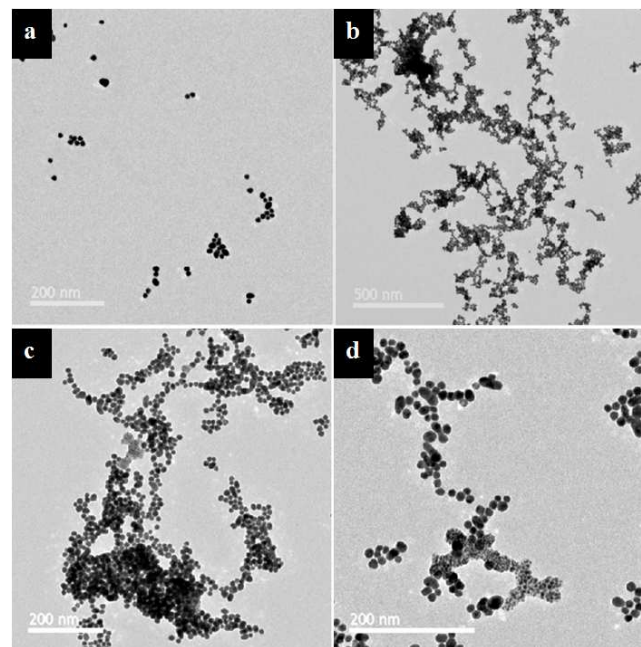


**Figure 15** TEM images showing the formation of aggregates of nanoparticles as acridine orange was added to a solution of gold nanoparticles: (a) 1 mL acridine orange added; (b) 3 mL acridine orange added; (c) 7 mL acridine orange added; (d) 10 mL acridine orange added.

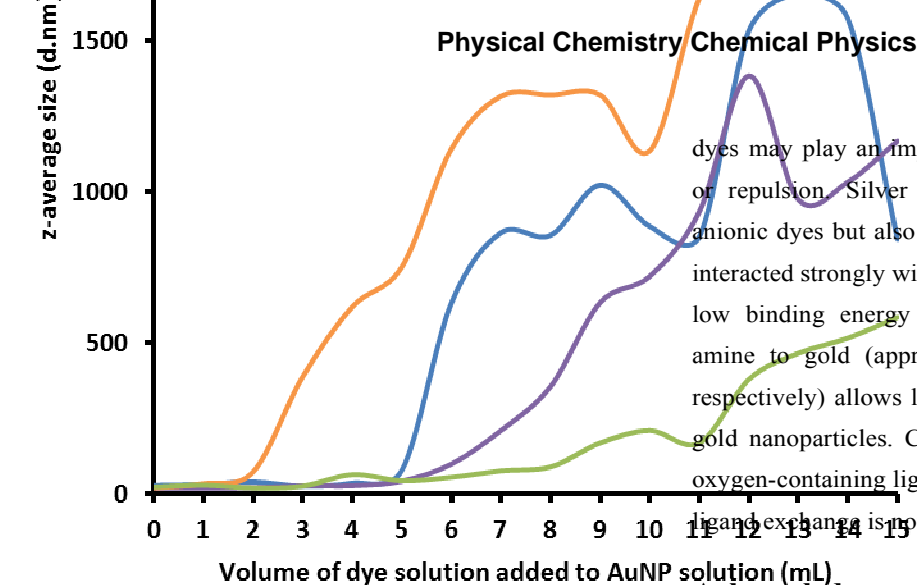


**Figure 17** Graph showing the increase in observed hydrodynamic radius of gold nanoparticles as dyes are added to the nanoparticle solution.

## Conclusions

It was found that all the cationic dyes interact strongly with a solution of gold nanoparticles and trigger aggregation of the nanoparticles into large arrays. This is accompanied by a new peak developing on the UV-vis spectra at a longer wavelength. Enhanced absorption of this peak was observed for toluidine blue, crystal violet and acridine orange. This phenomenon has been reported before for toluidine blue<sup>14</sup>, but not to the best of our knowledge for crystal violet or acridine orange. Anionic dyes did not produce aggregation or enhanced absorption. As anionic dyes don't trigger aggregation it can be concluded that agglomeration of the particles is not solely due to an increase in the anionic strength of the solution and that the charge on the

dyes may play an important part due to electrostatic attraction of repulsion. Silver nanoparticles show no interaction with anionic dyes but also no interaction with the cationic dyes that interacted strongly with gold nanoparticles. It is thought that the low binding energy of carboxylate to gold compared with amine to gold (approximately  $8 \text{ kJ mol}^{-1}$  and  $33 \text{ kJ mol}^{-1}$  respectively) allows ligand exchange to occur for gold nanoparticles. Conversely, silver will preferentially bind oxygen-containing ligands such as citrate over amine groups, so ligand exchange is not favourable in this case.

## Acknowledgements

The EPSRC are thanked for funding through the UCL Eng.D centre in Molecular Modelling and Materials Science. Heartfelt thanks also go to Joe Bear for help with TEM.

## References

1. B. Spellberg, R. Guidos, D. Gilbert, J. Bradley, H. W. Boucher, W. M. Scheld, J. G. Bartlett, J. Edwards and t. I. D. S. o. America, *Clinical Infectious Diseases*, 2008, **46**, 155-164.
2. T. J. Dougherty, C. J. Gomer, B. W. Henderson, G. Jori, D. Kessel, M. Korbelik, J. Moan and Q. Peng, *Journal of the National Cancer Institute*, 1998, **90**, 889-905.
3. G. Bertoloni, F. M. Lauro, G. Cortella and M. Merchat, *Biochimica et Biophysica Acta (BBA) - General Subjects*, 2000, **1475**, 169-174.
4. R. R. Allison, G. H. Downie, R. Cuenca, X.-H. Hu, C. J. Childs and C. H. Sibata, *Photodiagnosis and photodynamic therapy*, 2004, **1**, 27-42.
5. K. König, V. Bockhorn, W. Dietel and H. Schubert, *Journal of cancer research and clinical oncology*, 1987, **113**, 301-303.
6. J. Lopez, M. Carter, Y. P. Tsentlovich, O. Morozova, A. Yurkovskaya and P. Hore, *Photochemistry and photobiology*, 2002, **75**, 6-10.
7. P. S. Zolfaghari, S. Packer, M. Singer, S. P. Nair, J. Bennett, C. Street and M. Wilson, *BMC microbiology*, 2009, **9**, 27.
8. J. S. Bellin, L. Lutwick and B. Jonas, *Archives of Biochemistry and Biophysics*, 1969, **132**, 157-164.
9. K. Orth, G. Beck, F. Genze and A. Rück, *Journal of Photochemistry and Photobiology B: Biology*, 2000, **57**, 186-192.
10. A. C. Khazraji, S. Hotchandani, S. Das and P. V. Kamat, *The Journal of Physical Chemistry B*, 1999, **103**, 4693-4700.
11. A. Khair, B. Gerard, H. Handa, G. Mao, M. P. V. Shekhar and J. Panyam, *Molecular Pharmaceutics*, 2008, **5**, 795-807.
12. S. T. Naima Narband, Ivan P. Parkin, Jesús Gil-Tomás, Derren Ready, Sean P. Nair and Michael Wilson, *Current Nanoscience*, 2008, **4**, 409-414.
13. J. Turkevich, P. C. Stevenson and J. Hillier, *Discussions of the Faraday Society*, 1951, **11**, 55-75.

## Journal Name

14. N. Narband, M. Uppal, C. W. Dunnill, G. Hyett, M. Wilson and I. P. Parkin, *Physical Chemistry Chemical Physics*, 2009, **11**, 10513-10518.
15. Y. Wang, G. Chen, M. Yang, G. Silber, S. Xing, L. H. Tan, F. Wang, Y. Feng, X. Liu and S. Li, *Nature Communications*, 2010, **1**, 87.
16. D. V. Leff, L. Brandt and J. R. Heath, *Langmuir*, 1996, **12**, 4723-4730.
17. S. L. Westcott, S. J. Oldenburg, T. R. Lee and N. J. Halas, *Langmuir*, 1998, **14**, 5396-5401.
18. S. Bharathi, N. Fishelson and O. Lev, *Langmuir*, 1999, **15**, 1929-1937.
19. F. Chen, X. Li, J. Hihath, Z. Huang and N. Tao, *Journal of the American Chemical Society*, 2006, **128**, 15874-15881.
20. R. R. PR. Selvakannan , Blake J. Plowman , Ylias M. Sabri , Hemant K. Daima , Anthony P. O'Mullane , Vipul Bansal and Suresh K. Bhargava, *Physical Chemistry Chemical Physics*, 2013, **15**, 12920-12929.
21. T. Konno, M. Usami, A. Toyota, M. Hirotsu and T. Kawamoto, *Chemistry Letters*, 2005, **34**, 1146-1147.
22. N. Gonzalez-Lakunza, N. Lorente and A. Arnau, *The Journal of Physical Chemistry C*, 2007, **111**, 12383-12390.
23. D. Whitcomb and M. Rajeswaran, *Journal of Coordination Chemistry*, 2006, **59**, 1253-1260.
24. P. Lee and D. Meisel, *The Journal of Physical Chemistry*, 1982, **86**, 3391-3395.
25. L. M. Liz-Marzán, *Langmuir*, 2005, **22**, 32-41.